Available online at www.sciencedirect.com

ScienceDirect

Procedia Engineering 105 (2015) 520 – 528

Procedia Engineering

www.elsevier.com/locate/procedia

6th BSME International Conference on Thermal Engineering (ICTE 2014)

Flameless "Cool" Combustion in Multi-phase Configuration

Tanvir Farouk*

Department of Mechanical Engineering, University of South Carolina, Columbia, South Carolina, 29208, USA

Abstract

Cool flames are commonly associated with engine-knock phenomenon in spark ignition engines and autoignition in diesel engines, and results from low temperature partial oxidation of the fuel air mixture that eventually leads to hot flame ignition. However, the possibility of a cool flame supporting quasi-steady combustion of a fuel droplet has never been speculated, let alone been experimentally observed. Recent microgravity droplet combustion onboard the International Space Station (ISS) under the Flame Extinguishment (FLEX) Experiment Program showed anomalous combustion of *n*-heptane droplets; high temperature combustion followed by radiative visible extinction and a transition to a second stage burn characterized by loss of visible flame emission. In the second stage the droplet regression continues eventually resulting in extinction diameters characteristic of diffusive extinction. Experimental examples of the two stage burning and extinction characteristics of isolated *n*-heptane droplets under microgravity conditions are presented and analyzed numerically. Predictions show that the second stage combustion occurs as a result of chemical kinetics associated with classical premixed "*Cool Flame*" phenomena. In contrast to the kinetic interactions responsible for premixed cool flame properties, those important to cool flame droplet burning are characteristically associated with the temperature range between the turnover temperature and the hot ignition. Initiation of and continuing second stage combustion involves a dynamic balance of heat generation from diffusively controlled chemical reaction and heat loss from radiation and diffusion. Within the noted temperature range, increasing reaction temperature leads to decreased chemical reaction rate and vice versa. As a result, changes of heat loss rate are dynamically balanced by heat release from chemical reaction rate as the droplet continue to burn and regress in size. Factors leading to initiation of the second stage burning phenomena are also investigated. The chemical kinetics dictating the second stage combustion and extinction process is also discussed.

Peer-review under responsibility of organizing committee of the 6th BSME International Conference on Thermal Engineering (ICTE 2014)

Keywords: Droplet Combustion; Multi-stage Combustion; "Cool" Flames

* Corresponding author. Tel.: +1-803-777-3380; fax: +1-803-777-0106.
E-mail address: tfarouk@sc.edu

Peer-review under responsibility of organizing committee of the 6th BSME International Conference on Thermal Engineering (ICTE 2014)
doi:10.1016/j.proeng.2015.05.085

1. Introduction

Since 2009, the **Fl**ame **Ex**tinguishment (FLEX) Experiment has been conducting isolated droplet combustion experiments aboard the International Space Station (ISS). The overall goal of these experiments is to determine and analyze burning behavior, limiting oxygen index, and extinction mechanisms as a function of fuel, drop diameter, pressure, oxygen index, and dilution (using various diluents, including helium, nitrogen, and carbon dioxide) [1]. Unique to microgravity experiments is the ability to study a wide range of initial drop diameters so as to characterize both radiative and diffusive extinction phenomena. In the first phase of the program, methanol was utilized to obtain data on a non sooting fuel which absorbs combustion products over its burning history, notably water [1, 2]. More recently, the study of hydrocarbons was initiated using *n*-heptane as the fuel. In the case of methanol, classical diffusive and radiative extinction phenomena are observed, and a detailed numerical analysis of the results has recently appeared [2]. In the *n*-heptane experiments, radiative heat loss from larger diameter, ignited droplets results in cessation of classical (high temperature) droplet combustion behavior at a relatively large droplet size. In contrast to the classical radiative extinction observed with methanol, a transition to a second stage of low temperature constant burning rate behavior characterized by loss of visible flame emission follows; indicating an anomalous combustion characteristic. In this second stage the droplet continues to undergo rapid and apparent quasi-steady vaporization without the presence of a visible flame. This second stage burning and droplet regression continues, eventually resulting in diffusive extinction at a finite drop size that then apparently experiences additional time-dependent evaporation into the surrounding environment. This dual mode of combustion is only observed for sufficiently large initial droplet diameter; at smaller droplet diameters, classical single stage burning and high temperature diffusive extinction occurs.

Simulations are conducted to elucidate the influence of the coupled physico-chemical processes that triggers the observed dual-mode behavior. Simulations were conducted using a recently developed, one-dimensional, sphero-symmetric, transient combustion model [3]. The predictions from the model is compared against the recent ISS *n*-heptane droplet experiments [1]. Predictions from the model were found to compare favorably with the experimentally measured droplet and flame diameter evolution. Special attention is given to delineate whether the observed flames result from classical NTC, *"Cool Flame"* kinetic behavior or are other driving factors responsible for the dual-mode/two stage combustion process.

2. Mathematical Model

The mathematical model employed in this current work is a transient, spherosymmetric droplet combustion model featuring detailed gas phase kinetics, spectrally resolved radiative heat transfer and multi-component gas phase transport. Details of the model have been reported in some of our recent publications [2, 4]. A brief description of the model is provided here. The model comprises of species conservation for each of species considered and energy conservation in both the phases. The complete set of coupled partial differential and algebraic equations are discretized first in space and then integrated in an automated fashion as a set of coupled ordinary differential-algebraic equations in time. Spatial discretization is performed according to a node-centered finite volume scheme with a second order accuracy. The volume boundaries are defined to coincide with the liquid–gas interfacial and the far field (two hundred times the initial droplet diameter) boundary is well defined using Dirichlet conditions and remains fixed in the simulations. The Dirichlet conditions imposed on the far-field are of fixed ambient composition and temperature. The innermost liquid node is centered at the origin, providing the required no-flux condition. The discretized mass flux is represented on cell interfaces and not cell centers, in the manner traditionally referred to as a staggered grid to avoid oscillatory solutions. Numerical integration of the final set of discretized equations is performed using a backward difference formula with a variable order of up to fifth order and a variable time step utilizing a fully implicit multipoint interpolation. This makes it appropriate for the large range of time scales and stability constraints imposed by chemically reacting systems when combined with automatic time-step variation.

3. Results and Discussion

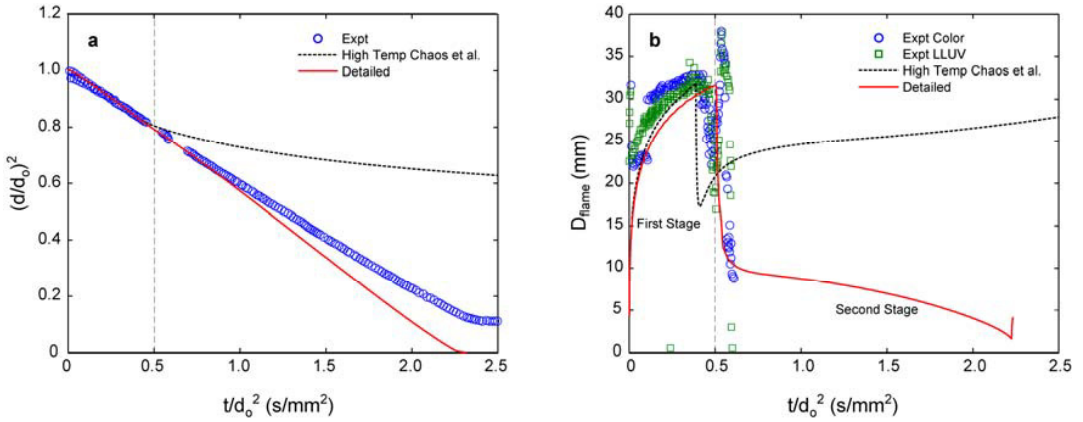

Fig. 1. Measured and predicted evolution of : (a) droplet diameter and (b) flame radius for a *n*-heptane droplet in ambient air (d_o = 3.91 mm, 0.21 X_{O2}, 0.79 X_{N2}, one atmosphere pressure). The experimental data are that of [1]. The flame radius experimental data contains measurement from both a color camera (Color) and low light UV (LLUV) camera. Predictions are shown with both the detail chemical kinetics model and the high temperature *n*-heptane model of Chaos et al. [5].

To get insight into the anomalous dual stage burning characteristics and hence affirm the combustion regime simulations were conducted with two chemical kinetics model, a "detailed" chemical kinetics model and a high temperature *n*-heptane chemical kinetic model [5] separately. It should be noted that the "high temperature" model of Chaos et al. was specifically developed for high temperature oxidation and did not include any low and intermediate temperature reaction pathways. Figure 1 shows the predicted droplet and flame diameter evolution from both these kinetic models and compares them to the experimental measurements [1]. The experimental conditions are d_o = 3.91 mm, 0.21 X_{O2}, 0.79 X_{N2}, one atmosphere pressure and is referred to as the base case. It can be seen that the predictions from the two kinetic models are distinctively different. The "high temperature" model predicts extinction of the droplet at a large droplet size due to radiative heat losses [2, 6] associated with the larger droplet size. After extinction the droplet is predicted to undergo evaporation in the quiescent environment, which is evident in the droplet diameter regression. Consistently the flame diameter evolution predictions with "high temperature" model shows an abrupt decrease corresponding to the flame extinction. In the simulations the peak temperature is utilized as the flame position marker as has been done some of our previous work. [2, 3]. As a consequence the flame diameter shows continuing evolution even after extinction. The "detailed" model shows significantly different combustion characteristics and captures the experimental observation qualitatively. The "detailed" model indicates that following the visible flame extinction which corresponds to the typical radiative extinction the droplet transitions to a second stage combustion where droplet diameter regresses at a significantly higher rate suggesting higher burning rate. In addition the "detailed" model predicts extinction towards the end of the second stage burn. During this second stage the flame diameter is found to be significantly smaller, locating itself very close to the droplet surface. Due to the large radiative heat loss (Figure 4) the flame positions itself closer to the droplet surface to compensate and sustain continuous burning. It can be seen that during the second stage the flame temperature is significantly lower and has a value of ~ 750K. The predictions from the "detailed" model are very similar to the "high temperature" model in the first stage the only difference being the temporal location of the transition. In comparison to the experiments the "high temperature" model shows an earlier extinction of the visible flame in contrast the "detailed" model predicts the transition to occur slightly later and is in good agreement with the experiments. Even though the "detailed" model qualitatively captures the experimental measurements, the second stage burning rate is significantly over predicted and vice versa for the extinction diameter. The predicted extinction diameter was found to be ~0.35 mm being smaller by a factor of 3.5 than the experiment.

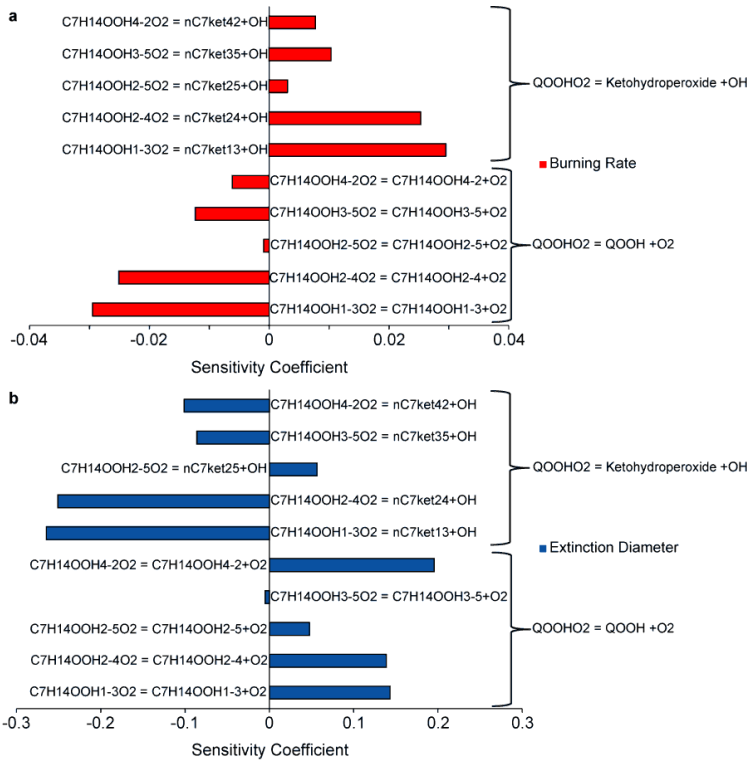

Fig. 2. Prominent sensitivity coefficients of (a) average burning rate $K_{b\,avg}$ and (b) extinction diameter d_{ext} on reaction rate coefficients (d_o = 3.91 mm, 0.21 X_{O2}, 0.79 X_{N2}, one atmosphere pressure).

The "detailed" model only provided qualitative agreement with the experimental measurement thus it is critical to obtain insight into the defining parameters of this discrepancy and at the same time determine the uncertainty limits of the predictions. The predictions from the "detailed" model showed very good agreement with the first stage measurement data. It is therefore the second stage combustion process that is not accurately predicted. As such simulations were conducted by perturbing each of the low temperature reactions individually (increase/decrease by a factor 2) to obtain the uncertainty bandwidth of the predictions and at the same time find out the sensitivity of the reactions to the average burning rate ($K_{b\,avg}$) and extinction diameter (d_{ext}). Figure 2 depicts the prominent sensitivity coefficients of droplet burning rate and extinction diameter on the reaction rates for the second stage burn. The sensitivity coefficient is identified as $S = \partial \log F(k) / \partial \log k = \partial F(k)\ k / \partial k\ F(k)$ where F is the target value which for this case is the average burning rate and extinction diameter. The sensitivity coefficient can be expressed by a finite difference formula, $S = [F(2k) - F(0.5k)]k / 1.5k\ F(k) = [F(2k) - F(0.5k)] / 1.5F(k)$, where the numerator represents the difference in the target value when the reaction rate is increased and decreased by a factor of two and the denominator denotes the target value for an unperturbed reaction rate. A positive sensitivity coefficient corresponds to a direct influence i.e. an increase in the parameter results in an increase in the target value and vice versa for negative sensitivity coefficient. The reactions having the most influence on the second stage burn was found to be isomerization of $QOOHO_2$ to ketohydroperoxide ($QOOHO_2 \rightarrow Ketohydroperoxide + OH$) and dissociation of $QOOHO_2$ ($QOOHO_2 \rightarrow QOOH + O_2$); Q = C_7H_{14} for this case. In general, increase in the rate of $QOOHO_2 \rightarrow Ketohydroperoxide + OH$ increased the burning and consequently decreased the extinction diameter. A vice versa is observed for the dissociation reactions. At temperatures lower than approximately 900K, the β - scission of alkyl radicals and internal H-atom abstraction reactions are slow to occur due to their high activation energies [7]. Under these conditions the most of the alkyl radicals (R) go through O_2 addition resulting in the formation of alkyl peroxy radicals RO_2. The alkyl peroxy radicals (RO_2) undergo isomerization to form QOOH which is the major pathway for the production of QOOH. The $QOOHO_2$ is formed by the addition of O_2 with

QOOH. At the low temperature regime the chain branching is mainly due to the reaction pathway leading through the ketohydroperoxide species. Hence the $QOOHO_2 \rightarrow Ketohydroperoxide + OH$ reactions have a positive effect on the second stage burning rate and vice versa for the extinction diameter. On the other hand the chain propagation reactions of QOOH species leads to the formation of cyclic ether, conjugate olefins and β decomposition products resulting in lower reactivity in the NTC regime. Therefore an increase in the $QOOHO_2$ dissociation rate to QOOH + O_2 decreases the second stage burning rate and accordingly increases the extinction diameter.

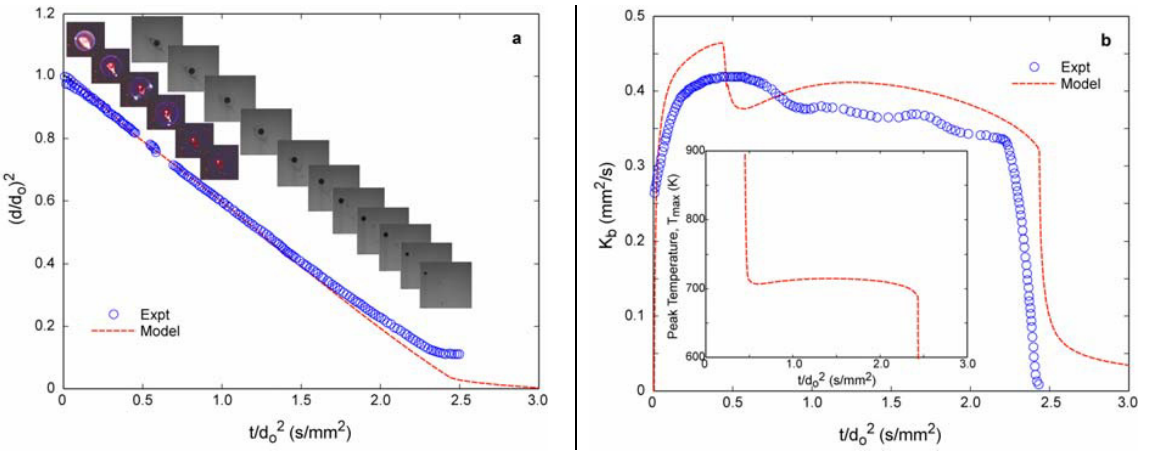

Fig. 3. Predicted evolution of (a) droplet diameter and (b) burning rate with the revised chemical kinetics model (d_o = 3.91 mm, 0.21 X_{O2}, 0.79 X_{N2}, one atmosphere pressure). Inset of experimental visualization of flame and droplet diameter is also provided which shows the continuing diameter regression after the flame extinguishment.

After identifying the most sensitive reactions for the second stage burn, simulations were conducted by modifying the reaction rates of these ten reactions to their uncertainty limit. For that the reaction rates for the $QOOHO_2 \rightarrow Ketohydroperoxide + OH$ reactions were decreased by a factor of 2 and the reaction rates for the $QOOHO_2 \rightarrow QOOH + O_2$ reactions were increased by a factor of 2. It should be noted though that the modification of these ten reaction rates is simply to observe their combined influence on the droplet combustion characteristics and it also brings forth the notion that the reaction rates for these ten reactions should be further investigated which is however not a scope of this work. Figure 3 presents the comparison of the measured and predicted droplet diameter and burning rate evolution utilizing the revised chemical kinetics model. It is evident that the predictions from the revised chemical kinetic model show better agreement with the measurements. The predicted average burning rate is obtained by time-averaging the instantaneous burning rate (K_o) between $t = 0.1t_b$ and $t = 0.95t_b$ where t_b is the total burn time (ignition to extinction). Comparing to the base kinetic model the revised chemical kinetics model predicts an average burning rate ($K_{b\,avg}$) of 0.385 mm^2/s and extinction diameter (d_{ext}) of 0.95 which is lower and higher by a factor of 1.15 and 2.38 respectively. In addition the second stage flame temperature is predicted to be~ 700 K by the revised kinetic model which is lower by 50 K than that of the base kinetic model predictions. However it should be noted that the model slightly over predicts the average burning rate and vice versa for the extinction diameter in comparison to the experimental measurements. The disparity between the two is most possibly a result of the well known perturbing effect of drift velocity. Ignition delay time and oxidation speciation predictions with the revised kinetic model were also found to be in improved agreement in the low and NTC temperature regime.

The integrated heat generation ($Q_{generation}$) and losses due to radiation ($Q_{radiation}$) and conduction ($Q_{conduction}$) are presented in Figure 4. Figure 4 shows that the integrated heat generation has a very sharp rise during ignition which also decreases very rapidly as a somewhat quasi-steady diffusion flame structure is established. The decrease in $Q_{generation}$ after ignition is also a consequence of the increasing radiative loss $Q_{radiation}$ during the first stage of the burn when the flame radius is still increasing (Figure 1). At the same time the conductive heat losses is also substantial. In this first stage of combustion the radiative heat loss is almost a factor of ~ 2 higher than the conductive losses. It can

be clearly seen that the transition to the second stage "*cool flame"* like behavior is initiated by the heat loss mechanism. The transition to the second stage occurs when the summation of the heat loss terms are close to the heat generation. As significant heat loss dominates the combustion process the flame positions itself close to the droplet surface for compensation as it is evident in Figure 3. During the second stage the $Q_{generation}$ is found to be ~ 17 W. On the basis of a time averaged heat generation rate of 150 W in the "high temperature" first stage the heat generation in the second stage is found to be ~ 11.5%. It is interesting to further note that during the second stage the dominant heat loss mechanism transforms to conduction from radiation. This is due to the fact that during the second stage as the flame is very close to the droplet surface the radiative heat loss decreases significantly.

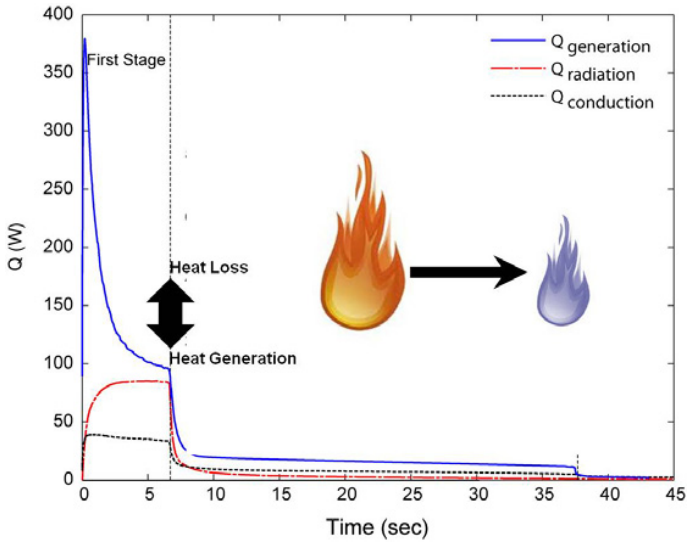

Fig. 4. Total heat generation, radiative and conductive heat losses for a *n*-heptane droplet undergoing two stage combustion in air (d_o = 3.91 mm, 0.21 X_{O2}, 0.79 X_{N2}, one atmosphere pressure).

More recent ISS *n*-heptane isolated droplet combustion experiments at three atmospheres pressure and the same oxygen index but with diluents inhibiting heat loss shows "multiple cycles" of dual stage combustion i.e. *hot – cool* flame transitions. The experiments are typically conducted for larger droplet sizes, d_o ~3 – 5 mm. For every experiment the combustion chamber is filled with the desired ambient gas mixture, consisting of oxygen, nitrogen and carbon dioxide to a pressure of 3.0 atm. In these experiments the flame steadily grows in diameter and decreases in luminous intensity to the point at which it reaches its maximum diameter where it then either suddenly extinguishes or begins to exhibit oscillatory behavior just prior to extinguishing. The oscillatory behavior is marked by repeated transitions between a complete and partial spherical flame surface and lasts for a brief period of time before completely extinguishing. The extinction of the visible flame commences the low temperature second stage burning regime, qualitatively referred to as the "*Cool Flame*" regime. During the second stage burning, rapid droplet vaporization persists and is only momentarily interrupted by the occurrence of one or more hot flame re-ignition events, typically lasting less than 1.0 s. The re-ignition event is initiated from a small region on the spherical surface that is eventually defined by a fully enveloping, re-ignited hot flame. This re-ignited high temperature flame has a diameter significantly larger than the preceding high temperature flame which had previously radiatively extinguished. An example of this re-ignition is provided in Figure 5 where a sequence of images taken 0.066 s apart shows the re-ignition kernel and the resulting flame wrapping around the contour of a spherical shell, presumably defining the stoichiometric surface. The re-ignited high temperature flame is not sustainable because, as with the original flame, its hypothetical flame radius without radiative loss exceeds that radius at which radiation loss exceeds heat generation.

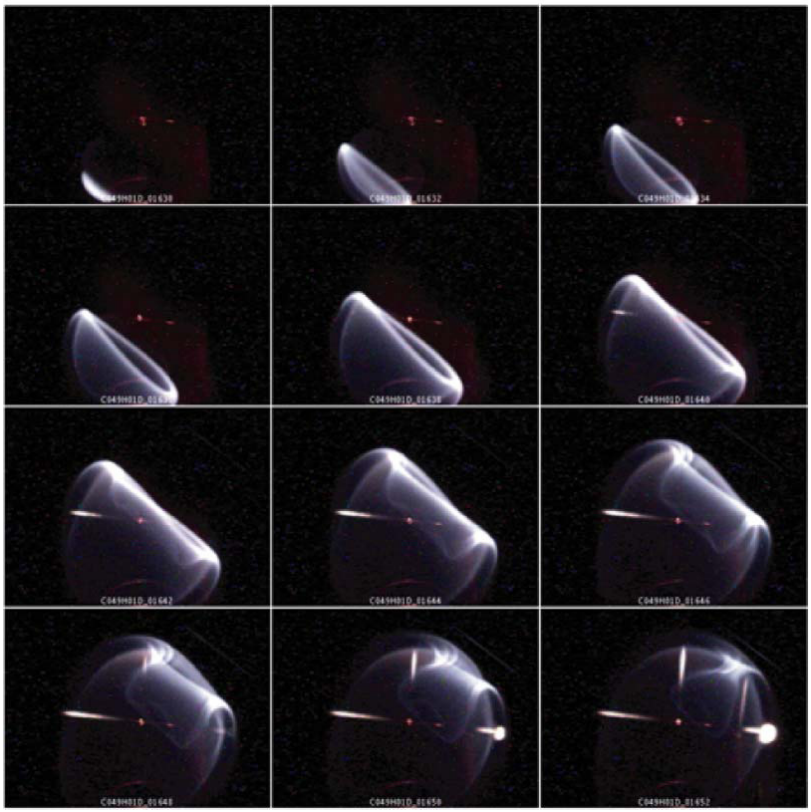

Fig. 5. Images showing the first of two spontaneous re-ignitions following a *second stage* combustion phase lasting approximately 10 s where no visible flame existed. Images in sequence are spaced 0.066 s apart and the total duration of the re-ignited hot flame is approximately 0.8 s. (d_o = 4.08 mm, 0.21 X_{O2}, 0.75 X_{CO2}/balance N_2, 3 atm)

Figure 6 shows the predicted droplet diameter and flame diameter evolution along with the experimental measurements. The experimental conditions are d_o = 4.08 mm, 0.21 X_{O2}, 0.75 X_{CO2}/balance N_2, at three atmosphere pressure. It can be seen that the predictions from the model agree favorably with the experimental measurement and captures all of the qualitative trends of the intricate features; especially the mutli-cycle two stage burning. The predicted droplet diameter regression rate is slower in comparison to the experiment. Likely experimental sources that may perturb the spherosymmetric result include slow gas/drop convection as a result of residual droplet drift [8] and movement along the tethering fiber, both of which may affect burning rate and the incomplete spherical flame structure/oscillatory behavior noted during transitions from low temperature burning to the second hot burning phase. It is apparent that in comparison to the atmospheric pressure experiments (Figure 1) the measured droplet diameter regression rates at elevated pressures show significantly greater departures from the local time averaged values. There exist multiple non-linear regimes in the droplet diameter regression rates. The flame diameter evolution presented in Figure 6b shows an example of this dynamic behavior. Initially the flame diameter is found to be large and together with the peak temperature evolution it is indicative of high temperature burning. Following the initial high temperature burn, the flame diameter is observed to decrease rapidly as a result of radiative heat loss, and transitions to the first low temperature/"*Cool Flame"* mode. Three subsequent initiations of transient hot flame burning of very short duration are each followed by a longer duration, *"Cool Flame"* burning period. In every *hot-cool flame* transition, the flame diameter is found to decrease by ~ 40- 50% of the prior cycle, maximum hot flame radius. Based on the predicted flame diameter evolution, the first transition to *"Cool Flame"* (i.e. visible flame extinction) is observed at t = 2.4 s, the first re-ignition at t_b = 4.64 s, the second and the third/last re-ignition

occuring at t_b = 14.56 s and t_b = 21.64 s. The predicted onset of second and third re-ignition that coincides with the experimentally observed 'first' and 'second' cases differs by ~ 2 s. However, the difference between the predictions and measurements during the very early stages ($0 \le t_b \le 5.0$ s) are likely the result of non-idealities in experiment and modeling of the experimentally aspherical, but symmetric hot wire ignition energy addition method. The initial ignition energy is known to significantly affect the transient establishment of the initial high temperature burning phase [9].

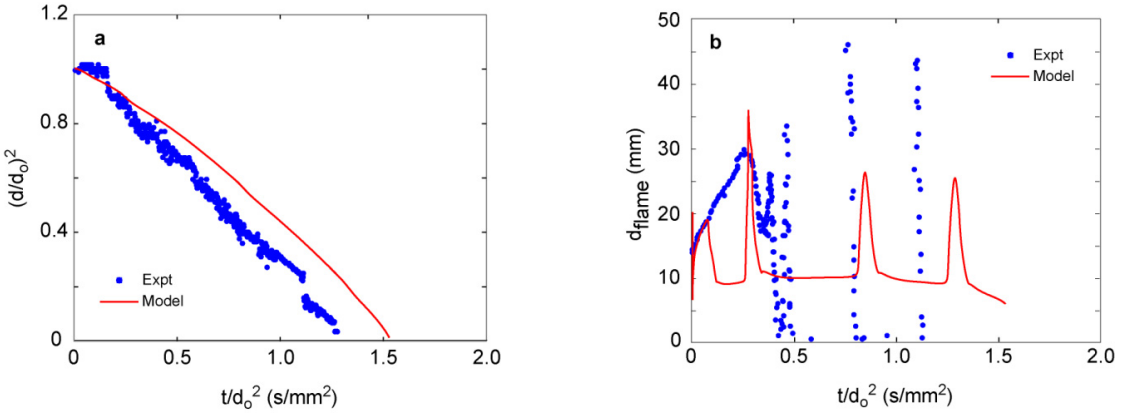

Figure 6. Measured and predicted evolution of: (a) droplet diameter and (b) flame diameter for a *n*-heptane droplet combustion. (d_o = 4.08 mm, 0.21 X_{O2}, 0.75 X_{CO2}/balance N_2, 3 atm).

4. Concluding Remarks

n-heptane droplet combustion under microgravity conditions has been successfully simulated using a recently developed transient spherosymmetric droplet combustion model. The simulation showed unique two stage "Cool Flame" like combustion behavior for large sized droplets. Unlike classical "Cool flames" these two stage combustion initiates at the high temperature combustion and then transitions to the "Cool flame" combustion process. The predictions from the simulations were found to be in good qualitative agreements with the experimental measurements The simulation results further indicated that heat losses initiates the two-stage behavior.

Acknowledgements

The work was supported by the National Aeronautics and Space Administration (NASA) through Grant Number NNX14AG461A.

References

[1] D. Dietrich, "Detailed results from the flame extinguishment experiment (FLEX)," *Technical Publication NASA/TP-2013-216046,* vol. NASA, Glenn Research Center, Cleveland OH 44135, USA, December 2013, 2013.
[2] T. I. Farouk and F. L. Dryer, "On the extinction characteristics of alcohol droplet combustion under microgravity conditions - A numerical study," *Combustion and Flame,* vol. 159, pp. 3208-3233, 2012.
[3] T. Farouk and F. L. Dryer, "Microgravity Droplet Combustion:Effect of Tethering Fiber on Burning Rate and Flame Structure," *Combustion Theory and Modelling,* vol. 15, pp. 487-515, 2011.
[4] T. Farouk and F. L. Dryer, "Tethered methanol droplet combustion in carbon-dioxide enriched environment under microgravity conditions," *Combustion and Flame,* vol. 159, pp. 200-209, 2012.
[5] M. Chaos, A. Kazakhov, Z. Zhao, and F. L. Dryer, "A high-temperature chemical kinetic model for primary reference fuels," *Int. J. Chem. Kinet.,* vol. 39, pp. 399-414, 2007.
[6] A. J. Marchese and F. L. Dryer, "The effect of non-luminous thermal radiation in microgravity droplet combustion," *Combustion Science and Technology,* vol. 124, pp. 371-402, 1997.
[7] H. J. Curran, P. Gaffuri, W. J. Pitz, and C. K. Westbrook, *Combustion and Flame,* vol. 114, pp. 149-177, 1998.
[8] M. Y. Choi, F. L. Dryer, and J. Haggard, "Observations of a slow burning regime for hydrocarbon droplets: n-heptane/air results,"

Proceedings of the Combustion Institute, vol. 23, pp. 1597 - 1604, 1990.

[9] T. Farouk, Y. C. Liu, A. J. Savas, C. T. Avedisian, and F. L. Dryer, "Sub-millimeter sized methyl butanoate droplet combustion: microgravity experiments and detailed numerical modeling," *Proceedings of the Combustion Institute,* vol. 34, pp. 1609 - 1616, 2013.